Three-magnon bound state in the quasi-one-dimensional antiferromagnet α-NaMnO2

Dally, Rebecca L.; Heng, Alvin J. R.; Keselman, Anna; Bordelon, Mitchell M.; Stone, Matthew B.; Balents, Leon; Wilson, Stephen D.

2020

Dally, R. L., Heng, A. J. R., Keselman, A., Bordelon, M. M., Stone, M. B., Balents, L., & Wilson, S. D. (2020). Three-magnon bound state in the quasi-one-dimensional antiferromagnet α-NaMnO2. Physical Review Letters, 124(19), 197203-. doi:10.1103/PhysRevLett.124.197203

https://hdl.handle.net/10356/145025

https://doi.org/10.1103/PhysRevLett.124.197203

Three-Magnon Bound State in the Quasi-One-Dimensional Antiferromagnet α-$NaMnO_2$

Rebecca L. Dally,[1,2,*] Alvin J. R. Heng,[3,4,*] Anna Keselman,[3] Mitchell M. Bordelon,[2] Matthew B. Stone,[5] Leon Balents,[3,†] and Stephen D. Wilson[2,‡]

[1]*NIST Center for Neutron Research, National Institute of Standards and Technology, Gaithersburg, Maryland 20899, USA*
[2]*Materials Department, University of California, Santa Barbara, California 93106, USA*
[3]*Kavli Institute for Theoretical Physics, University of California, Santa Barbara, Santa Barbara, California 93106, USA*
[4]*Division of Physics and Applied Physics, School of Physical and Mathematical Sciences, Nanyang Technological University, Singapore 637371, Singapore*
[5]*Neutron Scattering Division, Oak Ridge National Laboratory, Oak Ridge, Tennessee 37831, USA*

(Received 6 December 2019; accepted 29 April 2020; published 14 May 2020)

Here we report on the formation of a three-magnon bound state in the quasi-one-dimensional antiferromagnet α-$NaMnO_2$, where the single-ion, uniaxial anisotropy inherent to the Mn^{3+} ions in this material provides a binding mechanism capable of stabilizing higher order magnon bound states. While such states have long remained elusive in studies of antiferromagnetic chains, neutron scattering data presented here demonstrate that higher order $n > 2$ composite magnons exist, and, specifically, that a weak three-magnon bound state is detected below the antiferromagnetic ordering transition of $NaMnO_2$. We corroborate our findings with exact numerical simulations of a one-dimensional Heisenberg chain with easy-axis anisotropy using matrix-product state techniques, finding a good quantitative agreement with the experiment. These results establish α-$NaMnO_2$ as a unique platform for exploring the dynamics of composite magnon states inherent to a classical antiferromagnetic spin chain with Ising-like single ion anisotropy.

DOI: 10.1103/PhysRevLett.124.197203

One dimensional systems are renown for their ability to host ground states and phases markedly different from their higher dimensional counterparts. In the realm of magnetism, the prototypical $S = 1/2$ Heisenberg antiferromagnetic (AF) chain realizes a phase without order and power-law correlations, described at low energies by conformal field theory [1,2]. The corresponding $S = 1$ chain also avoids order, and hosts instead a topologically nontrivial Haldane-gapped state with protected $S = 1/2$ boundary spins [3,4]. While such quantum paramagnetic (i.e., not ordered) states in principle persist for any S in one dimension in the ideal case, they become increasingly fragile to perturbations as S increases and the semiclassical limit is achieved. In this regime, described by the nonlinear sigma model (NLSM) with a weak coupling of order $1/S$ [5], quantum fluctuations are confined to very low energies. A small anisotropy restricts those fluctuations to the "easy" directions, and for an Ising-like situation, this is sufficient to induce order.

Thus, large spin (e.g., $S \geq 2$) quantum spin chains seem an unlikely place to observe strongly quantum phenomena. Indeed this is true for their ground states; however, their excitations can still be highly quantum and realize interesting and paradigmatic few-body problems. Recent interest in few-body problems—i.e., the quantum mechanics of a finite number $n > 2$ of interacting particles [6]—stems largely from ultracold atoms, where examples include the formation of "droplets" of attractive bosons [7], and the Efimov states (three or more body bound states) in the unitary limit near a Feshbach resonance [8]. Generally this bound state formation is strongest in one dimension, and the multiple particle case is also known to be possible in spin chains from the study of field-induced multipolar orders in J_1-J_2 models [9]. In the latter case, the particles binding are magnons above a trivial field-induced polarized state [10], and lattice-scale competing interactions play an important role.

The cleanest, arguably most beautiful example of a few-body problem is the droplet mentioned above, which is a collection of one-dimensional bosons with attractive zero-range delta-function interactions. The fundamental physics of this problem is that increasing numbers of bosons bind more strongly, due to Bose statistics. Moreover, the ground state is, in this case, exactly soluble analytically via a simple application of the Bethe ansatz. In prior work, we uncovered a surprising connection of this canonical model problem to the large S nearest-neighbor antiferromagnetic chain with weak easy-axis Ising anisotropy [11]. The theory developed there predicts an approximate mapping of the quantum mechanics of magnons to the droplet problem of bosons. This mapping is nontrivial because the unperturbed NLSM is a gapless theory and, in it, binding would mean instability. Binding occurs as a subtle balance between fluctuations, weak anisotropy, and the intrinsic interactions of the NLSM.

In Ref. [11], the two-body bound state predicted by this theory was observed in the material α-$NaMnO_2$. Fundamentally, the crystal lattice of α-$NaMnO_2$ is built from two-dimensional sheets of triangular-lattice planes of Mn^{3+} moments, yet the Jahn-Teller effect inherent to the Mn-cations drives a coherent distortion of the triangular lattice into coupled isosceles triangles comprised of two long Mn-Mn distances and one short Mn-Mn exchange pathway [12]. This breaks the frustration of the triangular lattice and defines a strong AF nearest neighbor exchange energy (J_1) along the short bond length that defines the AF chain direction. Coupling between these chains is frustrated by equivalent AF next nearest neighbor couplings (J_2) via the two longer legs of the triangular lattice. The result is a highly one-dimensional spin system [13,14] with effective $J_1/J_2 = 8$ [11] that also possesses a weak Ising-like single-ion anisotropy, D, which we will estimate to be $D/J_1 = 0.086$. Magnon binding beyond two, however, has yet to be reported in this material or any other unperturbed antiferromagnet.

In this Letter, we present an acid test of the mapping of the spin lattice of α-$NaMnO_2$ to the droplet problem by uncovering a three-body bound state in α-$NaMnO_2$. Both $n = 2$ and $n = 3$ magnon bound states are observed in inelastic neutron scattering measurements with binding energies consistent with a minimal model of AF spin chains possessing an easy-axis uniaxial, single-ion anisotropy. To obtain the most accurate theoretical values for the bound state energies, we carry out numerically exact density matrix renormalization group and time evolution calculations, and compare with experiment. Our modeling suggests α-$NaMnO_2$ and other weakly anisotropic, large S chains can be excellent test platforms for few-body physics.

A single crystal of α-$NaMnO_2$ was grown via the floating zone method [15], and neutron scattering measurements were performed on the time-of-flight neutron spectrometer SEQUOIA [16] at the Spallation Neutron Source at Oak Ridge National Laboratory. The crystal was sealed in a cryostat with He exchange gas, and the (0,1,0) and (1,0,1) crystallographic directions were aligned in the horizontal scattering plane. Data were collected with incident neutron energies of $E_i = 30$ and 60 meV with the Fermi chopper in high-resolution mode, and the sample was rotated about the $[-1, 0, 1]$ axis in 1° increments over a range of 180°. Data were reduced and analyzed using the software package HORACE [17] and uncertainties where indicated represent plus and minus one standard deviation. Data are plotted as $I(\mathbf{Q}, E)$ corrected by k'/k. Throughout the paper, positions in momentum space, $\mathbf{Q}$, are reported in reciprocal lattice units (r.l.u.), where H, K, and L reflect $\mathbf{Q}[\text{Å}^{-1}] = [(2\pi/a \sin\beta)H, (2\pi/b)K, (2\pi/c \sin\beta)L]$ with $a = 5.63$ Å, $b = 2.86$ Å, $c = 5.77$ Å, and $\alpha = \gamma = 90°$; $\beta = 113°$.

Figure 1 shows inelastic neutron scattering data collected about the 1D AF zone center, (0, 0.5, 0), in the AF ordered state ($T = 4$ K). As the spin dynamics in this system are quasi-1D, data are integrated across the entire zone in H (the interchain) and L (the interplane) directions. The resulting color map of intensities plotted in Fig. 1(a) shows three branches of excitations dispersing along K (the intrachain direction), each of which are centered at the AF zone center $K = 0.5$ position. The first two branches are the previously identified single-magnon ($n = 1$) and two-magnon ($n = 2$) modes, and the third, highest energy branch suggests a higher order ($n > 2$) magnon bound state, which is the focus of this Letter.

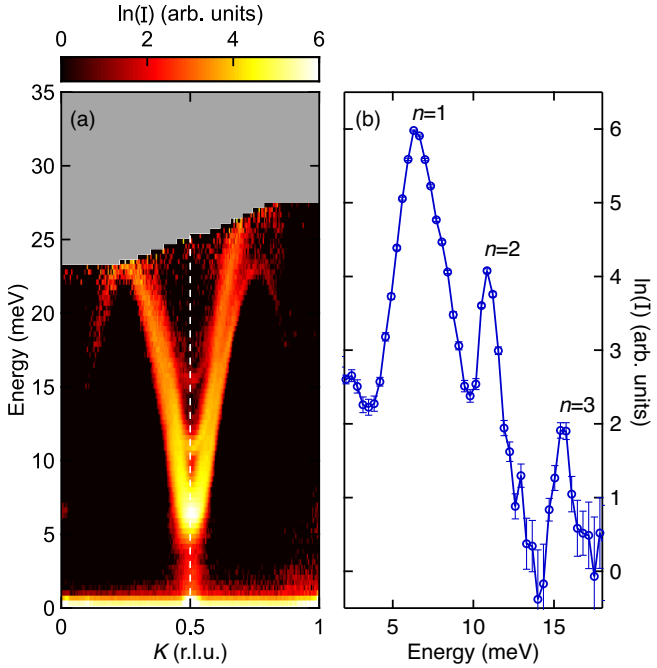

FIG. 1. Neutron scattering data collected with $E_i = 30$ meV at $T = 4$ K. The data were integrated throughout the entire zone in both H and L. (a) Intensity of the data on a logarithmic scale, where gray regions indicate no detector coverage. The dashed, white line shows the direction of the energy cut plotted in (b). (b) Energy cut through the intensity map centered at the AF zone center, $K = 0.5$, with the $n = 1$, $n = 2$, and $n = 3$ magnon modes.

To illustrate further, Fig. 1(b) shows an energy cut through the AF zone center. The lowest energy $n = 1$ mode appears at the expected zone center magnon gap near $E_1 = 6.15$ meV and is comprised of four, nearly degenerate modes superimposed from the two crystallographic and two magnetic twins inherent to this material. The second mode in Fig. 1, which is quasi-1D, is seen centered at $E_2 = 10.9$ meV and matches the energy of the previously reported, longitudinally polarized $n = 2$ bound state. Strikingly however, a third quasi-1D mode also appears at $E_3 = 15.5$ meV and, as we will show, corresponds to the formation of a native (zero field) three-magnon ($n = 3$) bound state.

We note here that because there is slight dispersion along the interchain direction, the full-width at half-maximum of

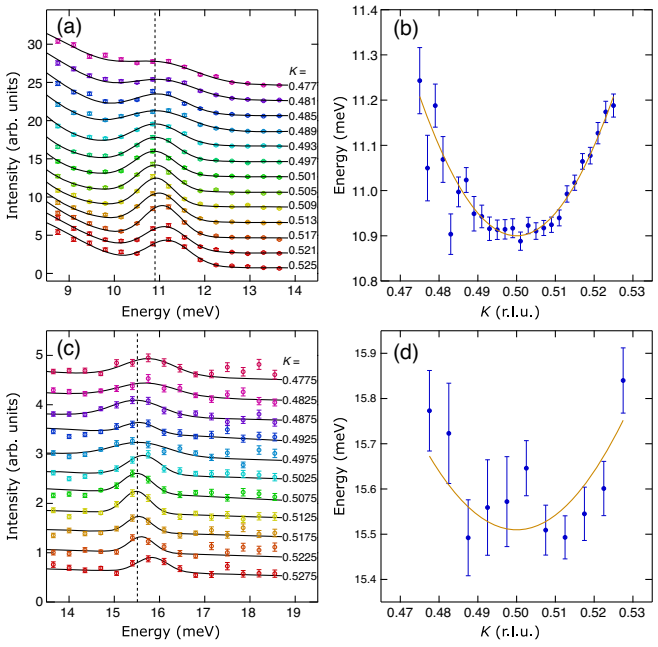

FIG. 2. Constant K cuts parametrizing the dispersions of the $n = 2$ and $n = 3$ modes. The data were integrated throughout the entire zone in both H and L and represent cuts through the color plot in Fig. 1. (a) Individual K cuts parametrizing the dispersion of the $n = 2$ mode. (b) Fit energies of the $n = 2$ mode plotted as a function of K. (c) Individual K cuts parametrizing the dispersion of the $n = 3$ mode. (d) Energies of the $n = 3$ mode as a function of K. The K cuts in panels (a) and (c) are offset from one another for clarity, and the solid black lines are fits parametrizing the modes' dispersions as described in the text. The solid orange lines in (b) and (d) are fits to the 1D dispersion described in the text. Error bars represent plus and minus one standard deviation.

the $n = 1$ mode appears broader than the energy resolution of the instrument (≈ 0.7 meV) due to the overlapping twins and momentum integration [11,18]. This twinning and integration, however, does not effect the $n = 2$ and $n = 3$ modes, which are inherently 1D and have nearly resolution limited full widths at half maxima in energy of 1.00 ± 0.01 meV and 0.74 ± 0.06 meV, respectively. Comparatively, the instrumental energy resolution at 10.9 meV is 0.64 meV and at 15.5 meV it is 0.58 meV. We provide additional evidence of their 1D nature in the Supplemental Material [19].

The dispersions of the $n = 2$ and $n = 3$ bound states are illustrated about the AF zone center via constant K cuts plotted in Figs. 2(a) and 2(c) (offset from one another for clarity). Fits parametrizing the energies of each mode as a function of K were performed using Gaussian peaks on a sloping background with the resulting mode dispersions shown in Figs. 2(b) and 2(d). Dispersion relations were then empirically quantified via a fit to the form $E(K) = \sqrt{\Delta^2 + c^2 \sin^2 2\pi K}$ with Δ reflective of the gap energy and c an empirical spin stiffness parameter.

For the $n = 2$ branch of excitations, Δ and c were found to be 10.900 ± 0.006 meV and 16.7 ± 0.4 meV, respectively. The dispersion of the higher energy $n = 3$ branch shown in Fig. 2(d) yields $\Delta = 15.51 \pm 0.03$ meV and $c = 16 \pm 2$ meV. While clear dispersion is evident in the data, parametrizing the effective spin-stiffness parameter for the $n = 3$ branch is coupled to the K bin size chosen. This is due to the weak nature of the $n = 3$ mode (which is nearly 2 orders of magnitude weaker than the $n = 1$ peak). Using the parametrization for the $n = 3$ mode shown in Fig. 2(d), the effective masses of the modes $m_i \propto \Delta/c^2$ have ratios of $m_1 : m_2 : m_3 = 1 : 3.5 : 5.4$.

The temperature dependence of the bound state modes is shown in Fig. 3. Energy cuts are plotted at three different temperatures: $T = 4$ K (in the AF ordered state), 30 K (in the incommensurate short-range ordered state), and 50 K (in the high temperature regime of quasi-one-dimensional correlations) [18]. True long-range order along the chains (divergent K-axis correlation lengths) occurs only below $T = 22$ K [18], and both $n = 2$ and $n = 3$ modes vanish above this temperature. The $n = 1$ single-magnon peak persists to high temperature as it becomes increasingly damped and broadens into the single-ion anisotropy gap with increasing temperature.

We now proceed to interpret the above results theoretically. Prior work on this compound developed a semiclassical theory to leading order in $1/S$ in the quasi-1D limit [11]. In that theory, $1/S$ corrections induce an attractive delta-function-like interaction between magnons, which creates the $n = 2$ two-magnon bound state. Within the same theory higher bound states are expected, as described in the Supplementary Material [19]. Here to obtain a more quantitative comparison with the experimental data that does not rely on the $1/S$ expansion, we carried out numerically exact matrix product state-based [21] calculations in the one-dimensional limit using the ITensor library [22].

Given the quasi-1D nature of α-$NaMnO_2$, in our numerical simulation we consider a $S = 2$ antiferromagnetic Heisenberg chain with single-ion anisotropy

$$H = J_1 \sum_j \vec{S}_j \cdot \vec{S}_{j+1} - D \sum_j (S_j^z)^2 \qquad (1)$$

where the sum over j indicates a sum over spins on a 1D lattice. We calculate the spectral function, which at zero temperature is given by

$$S(k, \omega) = \int_{-\infty}^{\infty} dt e^{i\omega t} \sum_{j=-\infty}^{\infty} e^{-ikj} \langle \vec{S}_j(t) \cdot \vec{S}_0(0) \rangle, \qquad (2)$$

where the expectation value is taken in the ground state of the system. We consider a finite chain with $N = 500$ sites and start by obtaining the ground state of the system using density matrix renormalization group (DMRG) [23]. We then perform time evolution up to times $t_{\max} = 20 J_1^{-1}$ using time evolving block decimation [19,24,25]. We note that

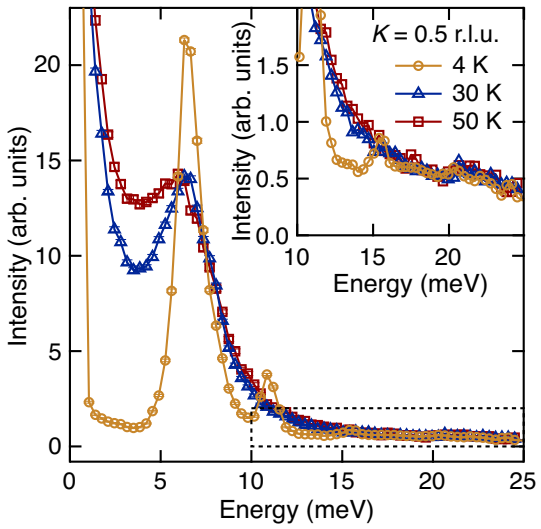

FIG. 3. $E_i = 30$ meV data showing the temperature dependence of spin excitations determined via an energy cut at the quasi-1D zone center, $\mathbf{Q} = (0, 0.5, 0)$. The inset shows a closeup in the region of the data, highlighting the temperature dependence of the $n = 3$ mode. Data are integrated across a width of 0.01 r.l.u. in K.

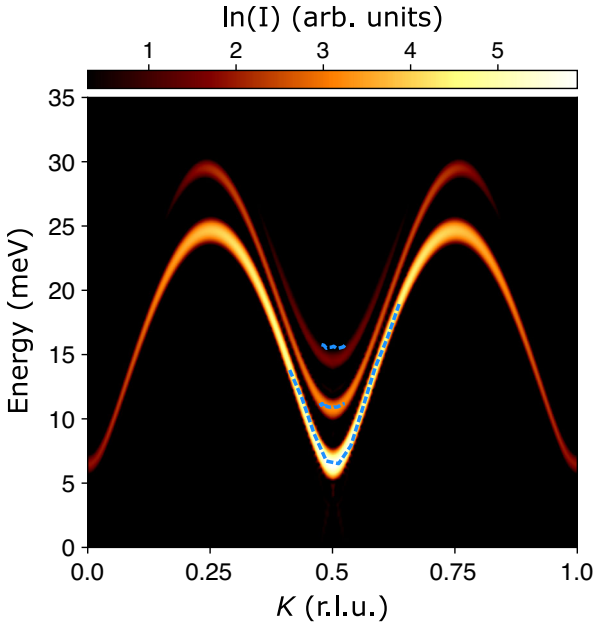

FIG. 4. Spectral function $S(K, E)$ obtained numerically using the 1D model, for $J_1 = 5.34$ meV and $D = 0.46$ meV. The intensity is normalized to a log scale. Three modes are clearly seen in the vicinity of $K = 0.5$. Blue dashed lines plotted on top correspond to dispersions obtained from experiment. The $n = 1$ data is obtained from a $(H, H, 0)$ cut, with integration in the L direction from $-0.5 < L(\text{r.l.u.}) < 0.5$ and integration in the $(-H, H, 0)$ direction from $-0.01 < H(\text{r.l.u.}) < 0.01$. The $n = 2$ and $n = 3$ data were obtained via cuts about the AF zone center from Fig. 1(b) and Fig. 2(c), respectively.

the spectral function intensities obtained from the numerical calculations are somewhat arbitrary because the magnitudes are related to how long in time they are simulated.

Using this model, we obtain an independent estimate for the couplings J_1 and D from a least squares fit of the dispersion of the $n = 1$ mode, obtained from the time-of-flight neutron experiment. The single-magnon mode momentum slice along the $(H, H, 0)$ direction (corresponding to a high-symmetry direction in the 3D reciprocal space) was modeled via the spectral function calculated numerically. This fit yields $J_1 = 5.34 \pm 0.08$ meV and $D = 0.46 \pm 0.02$ meV, roughly consistent with earlier estimates obtained from a fit to linear spin wave theory [19].

The spectral function obtained numerically for these values of J_1 and D is shown in Fig. 4, with the experimentally measured dispersions for the three modes plotted on top of it as blue dashed lines. The $n = 1$, $n = 2$, and $n = 3$ magnon modes are clearly visible in the spectral function in the vicinity of $K = 0.5$. The corresponding gaps are given by $E_1 = 6.4 \pm 0.4$ meV, $E_2 = 10.7 \pm 0.4$ meV, and $E_3 = 14.5 \pm 0.5$ meV.

We thus find a very good quantitative agreement with the aforementioned experimental values for the gaps of the $n = 2$ and $n = 3$ modes without further fitting parameters. The success of this purely 1D theory is also consistent with the observation that these higher order modes are dispersionless along both the interchain and interplane directions. We note here that the unbound multimagnon continuum typically present in quasi-1D systems is strongly suppressed due to spectral weight transfer into the $n = 2$ and $n = 3$ bound states. A weak continuum is resolved in our spectral function calculation [19]; however, its intensity is well outside of the resolution of the experimental data.

A physical interpretation of the bound states is as follows. The elementary excitations of the system (which comprise the E_1 mode) are magnons, which behave as massive relativistic particles. These come in two "flavors," with spin $S^z = \pm 1$ along the Ising axis. The E_2 mode arises as a bound state of two unlike particles, and hence carries $S^z = 0$, which is why it is longitudinal. The third E_3 mode corresponds to a bound state of two like and one unlike particles, e.g., two $S^z = +1$ and one $S^z = -1$ magnons (or vice versa), which gives it a total $S^z = \pm 1$ implying it is transverse. Our data indeed show this to be the case, and by tracking the intensity of the mode as a function of momentum about the zone center, the geometric factor contribution is qualitatively consistent with a transversely polarized mode [19]. The analytic treatment in the strict $1/S$ expansion discussed in the Supplemental Material further confirms the presence of these bound states,[19] though the DMRG calculations are more quantitative. Multiple magnon binding in $NaMnO_2$ is therefore a remarkable and unexpected manifestation of new physics accessible in higher spin one-dimensional chains.

In summary, we have shown that the quasi-1D spin dynamics endemic to the anisotropic triangular lattice of $NaMnO_2$ manifest a series of long-lived, high order magnon bound states, providing for the seminal observation of a

native $n = 3$ three-magnon bound state in an antiferromagnet. This result is captured by a semiclassical theory of interacting magnons within a 1D chain weakly bound by uniaxial single-ion anisotropy, which effectively maps to few-body droplet models of interacting bosons bound via weak delta function potentials. Therefore $NaMnO_2$, and we propose likely other anisotropic triangular antiferromagnets with weak, Ising-like single ion anisotropy, are appealing platforms for exploring few-body interactions in a condensed matter setting.

This work was supported by DOE, Office of Science, Basic Energy Sciences under Award No. DE-SC0017752 (S. D. W., R. D., and M. B.). Work by L. B. was supported by the DOE, Office of Science, Basic Energy Sciences under Award No. DE-FG02-08ER46524. This research is funded in part by the Gordon and Betty Moore Foundation to support the work of A. K. through Grant No. GBMF8690 to UCSB. A. J. R. H. thanks the Nanyang Technological University for financial support through the CN Yang Scholars Program. M. B. also received partial support from the National Science Foundation Graduate Research Fellowship Program under Grant No. 1650114. Use was made of the computational facilities administered by the Center for Scientific Computing at the California Nanosystems Institute (CNSI) and Materials Research Lab (MRL) (an NSF Materials Research Science and Engineering Center (MRSEC); DMR-1720256) and purchased through NSF CNS-1725797. A portion of this research used resources at the Spallation Neutron Source, a DOE Office of Science User Facility operated by the Oak Ridge National Laboratory.

*Contributed equally to this work.
†balents@kitp.uscb.edu
‡stephendwilson@uscb.edu

[1] F. D. M. Haldane and M. R. Zirnbauer, Phys. Rev. Lett. **71**, 4055 (1993).
[2] S. Eggert, I. Affleck, and M. Takahashi, Phys. Rev. Lett. **73**, 332 (1994).
[3] F. D. M. Haldane, Phys. Rev. Lett. **50**, 1153 (1983).
[4] I. Affleck, J. Phys. Condens. Matter **1**, 3047 (1989).
[5] F. D. M. Haldane, Phys. Lett. **93A**, 464 (1983).
[6] D. C. Mattis, Rev. Mod. Phys. **58**, 361 (1986).
[7] Y. Sekino and Y. Nishida, Phys. Rev. A **97**, 011602(R) (2018).
[8] M. Zaccanti, B. Deissler, C. D'Errico, M. Fattori, M. Jona-Lasinio, S. Müller, G. Roati, M. Inguscio, and G. Modugno, Nat. Phys. **5**, 586 (2009).
[9] J. Sudan, A. Lüscher, and A. M. Läuchli, Phys. Rev. B **80**, 140402(R) (2009).
[10] L. Kecke, T. Momoi, and A. Furusaki, Phys. Rev. B **76**, 060407(R) (2007).
[11] R. L. Dally, Y. Zhao, Z. Xu, R. Chisnell, M. B. Stone, J. W. Lynn, L. Balents, and S. D. Wilson, Nat. Commun. **9**, 2188 (2018).
[12] M. Giot, L. C. Chapon, J. Androulakis, M. A. Green, P. G. Radaelli, and A. Lappas, Phys. Rev. Lett. **99**, 247211 (2007).
[13] A. Zorko, S. El Shawish, D. Arčon, Z. Jagličić, A. Lappas, H. van Tol, and L. C. Brunel, Phys. Rev. B **77**, 024412 (2008).
[14] C. Stock, L. C. Chapon, O. Adamopoulos, A. Lappas, M. Giot, J. W. Taylor, M. A. Green, C. M. Brown, and P. G. Radaelli, Phys. Rev. Lett. **103**, 077202 (2009).
[15] R. Dally, R. J. Clément, R. Chisnell, S. Taylor, M. Butala, V. Doan-Nguyen, M. Balasubramanian, J. W. Lynn, C. P. Grey, and S. D. Wilson, J. Cryst. Growth **459**, 203 (2017).
[16] G. E. Granroth, A. I. Kolesnikov, T. E. Sherline, J. P. Clancy, K. A. Ross, J. P. C. Ruff, B. D. Gaulin, and S. E. Nagler, J. Phys. Conf. Ser. **251**, 012058 (2010).
[17] R. Ewings, A. Buts, M. Le, J. van Duijn, I. Bustinduy, and T. Perring, Nucl. Instrum. Methods Phys. Res., Sect. A **834**, 132 (2016).
[18] R. L. Dally, R. Chisnell, L. Harriger, Y. Liu, J. W. Lynn, and S. D. Wilson, Phys. Rev. B **98**, 144444 (2018).
[19] See Supplemental Material at http://link.aps.org/supplemental/10.1103/PhysRevLett.124.197203, which includes Ref. [20], for supporting theoretical analysis and additional neutron scattering data.
[20] S. R. White and I. Affleck, Phys. Rev. B **77**, 134437 (2008).
[21] U. Schollwöck, Ann. Phys. (Amsterdam) **326**, 96 (2011).
[22] ITensor Library, http://itensor.org/.
[23] S. R. White, Phys. Rev. Lett. **69**, 2863 (1992).
[24] G. Vidal, Phys. Rev. Lett. **91**, 147902 (2003).
[25] G. Vidal, Phys. Rev. Lett. **93**, 040502 (2004).